Separation and Purification Technology 353 (2025) 128281

Contents lists available at ScienceDirect

Separation and Purification Technology

journal homepage: www.elsevier.com/locate/seppur

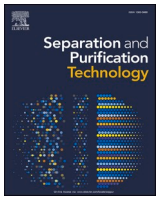

Integrating diffusion dialysis for sustainable acid recovery from ion exchange regeneration stages: Characterization of metal and non-metal ions migration

V. Vallès [a,b,*], M. Fernández de Labastida [a,b], S. Randazzo [c], A. Cipollina [c], D. Winter [d], J. Koschikowski [d], J. López [a,b], J.L. Cortina [a,b,e]

[a] Chemical Engineering Department, Escola d'Enginyeria de Barcelona Est (EEBE), Universitat Politècnica de Catalunya (UPC)-BarcelonaTECH, C/ Eduard Maristany 16, Campus Diagonal-Besòs, 08019 Barcelona, Spain
[b] Barcelona Research Center for Multiscale Science and Engineering, C/ Eduard Maristany 16, Campus Diagonal-Besòs, 08019 Barcelona, Spain
[c] Dipartimento di Ingegneria, Università di Palermo (UNIPA), Viale delle Scienze ed. 6, 90128 Palermo, Italy
[d] Fraunhofer Institute for Solar Energy Systems ISE, Heidenhofstraße 2, Freiburg im Breisgau 79110, Germany
[e] CETaqua, Carretera d'Esplugues, 75, 08940 Cornellà de Llobregat, Spain

ARTICLE INFO

Editor: Gaohong He

Keywords:
Diffusion dialysis
Ion exchange
Acid recovery
Brine
Fumasep FAD-PET-75
Anion exchange membrane

ABSTRACT

Seawater mining presents a potential option for recovering the European Union's Critical Raw Materials (CRMs), but direct extraction from seawater is challenging due to their low concentrations, as most of them are Trace Elements (TEs) (at levels of mg/L or μg/L). Saltworks *bitterns* (ultraconcentrated brines resulting from the sea salt production process) offer an alternative solution, naturally concentrated up to 40 times more than seawater. These bitterns can be further processed with chelating Ion Exchange (IX) sorbents to selectively extract TEs. However, this process requires an acidic elution stage with strong acids, followed by neutralization, to recover TEs through precipitation, demanding extensive chemicals consumption. Diffusion Dialysis (DD) could be used to recover the excess acid without external reagents, using an acid-resistant Anion Exchange Membrane (AEM). This study evaluates DD through batch and once-through tests for acid recovery from simulated IX eluate generated in the elution stage of TEs (B, Ga, Ge, Co, Sr) recovery from saltworks bitterns.

Batch tests achieved high recoveries for HCl (45–50 %) and H_2SO_4 (30–37 %), being the theoretical maximum attainable recovery equal to 50 %. B and Ge only partially permeated through the membrane (82 % rejection) by a diffusion mechanism in their neutral form (H_3BO_3(aq), H_4GeO_4(aq)). Ga, Co and Sr, in cationic form, were highly rejected (>96 %). Permeability followed the order Ga < Sr < Co ≪ Ge < B, due to the relevant charge and size. HCl permeability correlated linearly with concentration, while H_2SO_4 was inversely proportional. Once-through tests showed higher acid (74 % HCl, 62 % H_2SO_4) and oxoacid (66 % H_3BO_3(aq), 52 % H_4GeO_4(aq)) recovery at a low specific flow rate, or apparent flux, (0.38 L/($m^2_{membrane}$·h)) due to increased residence time. Water to acid flow rate ratios did not affect species transport when an excess of water was guaranteed. Conversely, an influence was observed when the ratio was below 1, with a minimum at 0.18, where a very low passage of species was observed due to the reduced dilution volume of the dialysate solution (water). A 1D transport model, incorporating the solutes permeabilities determined experimentally, effectively described the system performance, especially for HCl and B, albeit slightly overestimating the other TEs' transport.

1. Introduction

Seawater mining is considered as one of the main alternative sources to recover raw materials from an infinitely abundant resource, such as seas and oceans, and it is currently used to extract major elements, such as Na, K and Mg [1–3]. Apart from them, certain elements of interest, classified as Critical Raw Materials (CRMs) by the European Union (EU) [4], are not feasible to be extracted directly from seawater due to their

* Corresponding author at: Chemical Engineering Department, Escola d'Enginyeria de Barcelona Est (EEBE), Universitat Politècnica de Catalunya (UPC)-BarcelonaTECH, C/ Eduard Maristany 16, Campus Diagonal-Besòs, 08019 Barcelona, Spain.
E-mail address: victor.valles.nebot@upc.edu (V. Vallès).

https://doi.org/10.1016/j.seppur.2024.128281
Received 22 March 2024; Received in revised form 30 April 2024; Accepted 2 June 2024
Available online 4 June 2024

low concentration (namely Trace Elements (TEs)), being in some cases in the order of μg/L (e.g., Co, Ga, Ge) [5,6]. Due to the economic importance of these CRMs to the EU economy, their extraction is being pursued from more concentrated brines, as in the case of Seawater Reverse Osmosis (SWRO) brines [7] or *bitterns* [8], which are produced in the sea salt production facilities, named saltworks, as a by-product of the final NaCl crystallization step [9,10]. Contrary to SWRO, where the elements can be concentrated roughly by a factor of 2, the bitterns exhibit concentration factors up to 40 [8], making the recovery of TEs more technically and economically feasible.

According to the literature, the recovery of TEs can be achieved by using Ion Exchange (IX) or sorption technologies, because of their low-cost operation, high selectivity and long lifetime and stability [11–14]. Recently, Vallès et al. [15] evaluated the recovery of B from bitterns using N-methylglucamine-based resins (Purolite S108 and Diaion CRB03 and CRB05). The authors reported the possibility to concentrate B by factors up to 7.5 for S108 and up to 9.6 for CRB05 after elution with 1 mol/L HCl. In a later work, Vallès et al. [16] evaluated both polymeric and inorganic sorbents for TEs (Co, Ga, Ge, Rb, Sr, Cs) recovery from bitterns. The authors reported concentration factors up to 710 for Co with IRC747 and S940 using 1 mol/L HCl during elution. However, the concentration achieved in the eluate can limit the subsequent recovery of TEs in solid form, even though the high concentration factors achieved during IX extraction. In fact, solids might get polluted with NaCl during crystallization due to the need to neutralize the eluate to recover the solids as hydroxides [17]. Therefore, the acid must be removed prior to any crystallization step.

Diffusion Dialysis (DD) stands out in the removal of acidity without the need of any external reagent. This process comprises an Anion Exchange Membrane (AEM), which presents a positively charged membrane surface that impedes the transport of cations, while allowing strong acid permeation (e.g., HCl, H_2SO_4, HNO_3) [18,19]. DD has been widely studied for acid recovery and purification. When working in HCl media, it was possible to recover acid more than 80 % using either waste pickling solutions, extremely rich in heavy metals [20], or galvanizing wastes [21]. In both cases, the membrane was able to quantitatively block iron ions (transport below 15 %), but around 50–60 % of the Zn permeated because of the presence of anionic metal-chloride complexes (e.g., $ZnCl_3^-$ and $ZnCl_4^{-2}$) [20,22]. With respect to H_2SO_4 recovery, similar outcomes were observed. Sulphuric acid was successfully recovered (>75 %) working with different solutions, being waste streams from electroplating processes [23], off-gases treatment waters produced in Cu smelters [24], to remove traces of metals from sulphuric acid streams [25], and from battery wastewater [26]. It was observed that acid recovery decreased with its concentration [23], whereas working at higher temperature can enhance its recovery [25]. In relation to the removal of metallic impurities, they were removed by more than 96 % [23,25,26] because of charge exclusion, but if neutral species are present in solution (e.g., arsenic as H_3AsO_3(aq)/H_3AsO_4(aq)) they permeated freely across the membrane (around 40 %) [24].

Even though most of the published studies are focused on metallurgy industries, none of them proposes the integration of DD for acid recovery from the streams generated in metal recovery and concentration stages using IX sorbents. Apart from that, published studies collect data on the rejection of metallic species in the order of g/L, without emphasis on compounds at levels of mg/L or oxoacids, typically present in acidic solutions as non-charged species.

In this work, DD with AEM (Fumasep FAD-PET-75) was evaluated to recover the acidity from solutions that simulate the eluate of IX resins used to recover TEs (B, Ge, Ga, Co and Sr) from saltworks bitterns. Initially, batch tests were carried out to assess the transport of species across the AEM based on the concentration and solutes speciation (strong acids (e.g., HCl, H_2SO_4), weak oxoacids (e.g., H_3BO_3(aq), H_4GeO_4(aq)) and cations). The data was used to infer membrane permeabilities to species through the use of a 1D model based on convective and diffusive transport equations, accounting for both boundary layers and membrane resistance. Finally, membrane performance was also evaluated in a once-through test cell, aiming to evaluate the effect of specific flow rate and flow rate ratio (water to acid) on acid recovery and metal leakage. The data derived from the once-through test cell was later used to validate the mathematical model using the previously determined membrane permeabilities in batch tests.

2. Materials and methods

2.1. Chemicals

Experiments were conducted with synthetic solutions, which were prepared stating from deionised water, 37 % HCl (Sigma-Aldrich) and 96 % H_2SO_4 (PanReac) solutions, $CoCl_2{\cdot}6H_2O$ (>98 %, Alfa Aesar), $SrCl_2{\cdot}6H_2O$ (>98 %, Alfa Aesar), H_3BO_3 (>99.5 %, Sigma-Aldrich), Ga plasma standard solution (10,000 mg/L, Alfa Aesar) and Ge plasma standard solution (10,000 mg/L, Alfa Aesar). In addition, for analytical purposes, 69 % HNO_3 (PanReac) solution and NaOH (98 %, PanReac) were also employed. Milli-Q water (Synergy UV) was used in the samples' preparation for analysis.

2.2. Solution composition and diffusion dialysis set-up

Two different operational set-ups (Fig. 1) were used to carry out batch and once-through experiments.

Batch tests (Fig. 1.a) were performed with a plate and frame DD unit, consisting of two Teflon plates of 21x16.5x3.7 cm^3 containing inlet–outlet manifolds, two spacers (0.081 cm thickness) and an AEM allocated between the spacers, with an active area of 12.0x7.1 cm^2. The acid feed and water solutions were pumped through the set-up by a D-25VXi peristaltic pump (DINKO Instruments) providing a flow rate of 100 mL/min.

Once-through experiments (Fig. 1.b) were conducted using an AP-L05 Diffusion Dialysis Lab Unit (Mech-Chem, USA), equipped with an acid (feed) and a water tank connected to two metering pumps, which impel the solutions in a counter-current regime to a plate and frame stack of 8 membrane sheets (active area of 7.62x15.24 cm^2) providing a total area of 929 cm^2. Tests were performed adopting the once-through configuration aimed to evaluate the acid and water specific flow rate (0.38–3.26 L/(m^2·h)) and the flow rate ratio ($0.18 \leq Q_{Water}/Q_{Feed} \leq 1.84$) effect on the transport of species. The main objective of these experiments was to achieve the highest acid recovery with the lowest migration of TEs.

All experiments were performed with Fumasep FAD-PET-75 AEMs, containing ammonium quaternary groups, with a thickness of 70–80 μm, an anion exchange capacity of 2.0–2.3 meq/g and a resistance of 0.25–0.50 Ω·cm^2 [27]. Membranes were previously conditioned in 1.5 % NaCl solution for 24 h.

Experiments performed with the batch set-up can be distributed in four sets of tests, according to the feed solutions used, some of which mimicked the composition of eluate solutions obtained in typical IX elution stage, as already analysed in previous research works of some of the authors: (i) pure HCl solutions; (ii) HCl and H_2SO_4 mixture; (iii) HCl and H_2SO_4 mixture containing oxoacids (B, Ga and Ge); and (iv) HCl and H_2SO_4 mixture containing metallic cationic species (Co and Sr). The concentration values on acids were selected with the objective to evaluate the dependence of acid transport on its initial concentration. In the case of TEs, the different levels were selected based on previous IX studies [15,16], where it was possible to concentrate the different TEs (Co, Ga, Ge) by factors up to 150, Sr by a factor up to 10 and B by factors within 10–20. Once-through tests were conducted with a fixed feed solution composition, also mimicking the eluate effluent from IX columns determined in previous research.

Table 1 provides a summary of feed solutions composition adopted in the tests performed.

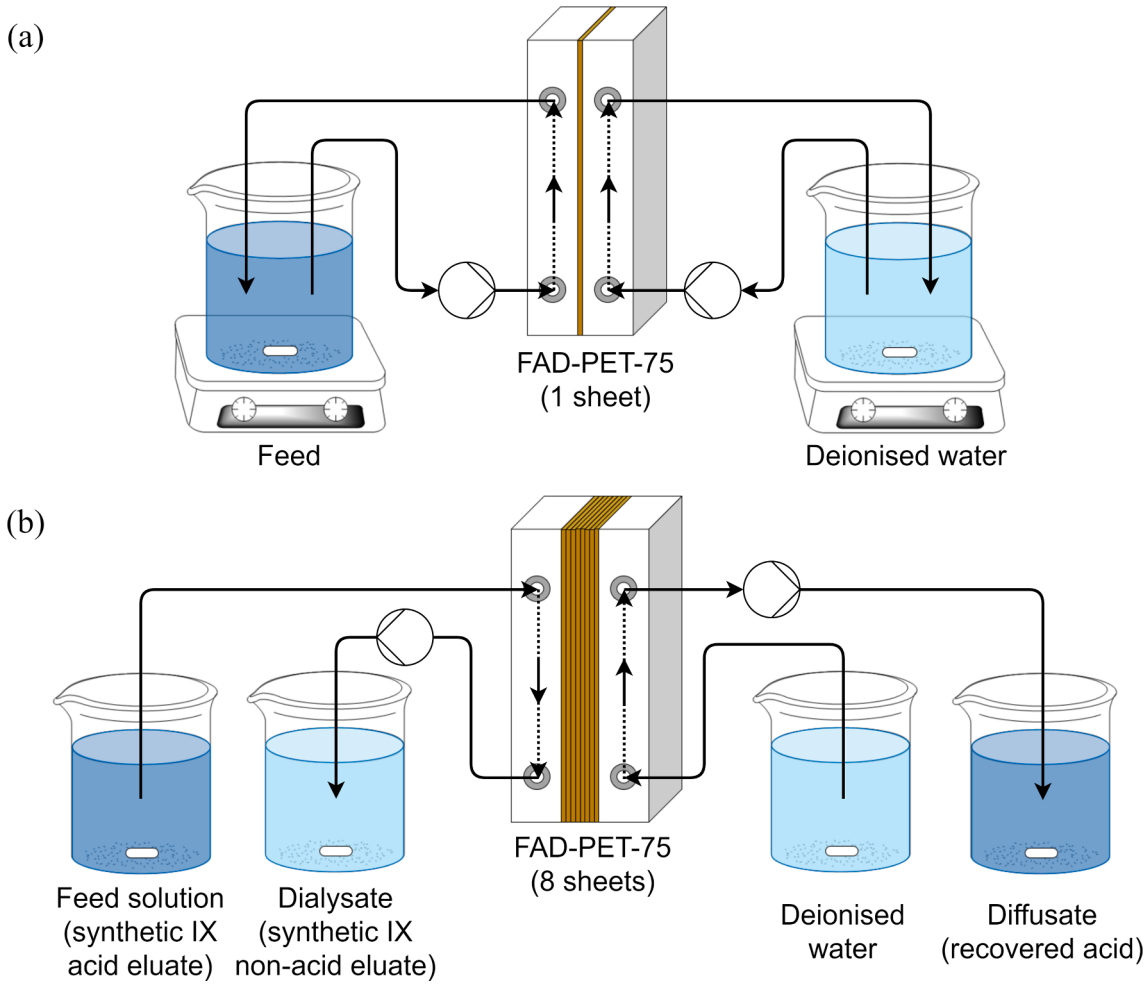

Fig. 1. Schemes of the set-up used for (a) batch and (b) once-through experiments.

Table 1
Composition of the feed solutions used. Experiments #1–13 were conducted as batch tests, while all the once-through experiments were carried out with the same solution.

Experiment	Acids (mol/L)		Elements (mg/L)				
	HCl	H_2SO_4	B	Ga	Ge	Co	Sr
1	0.25	–	–	–	–	–	–
2	0.50	–	–	–	–	–	–
3	0.75	–	–	–	–	–	–
4	1	–	–	–	–	–	–
5	1	0.05	–	–	–	–	–
6	1	0.10	–	–	–	–	–
7	1	0.20	–	–	–	–	–
8	1	0.10	500	13	5	–	–
9	1	0.10	1000	25	10	–	–
10	1	0.10	2000	50	20	–	–
11	1	0.10	–	–	–	50	50
12	1	0.10	–	–	–	100	100
13	1	0.10	–	–	–	200	200
Once-through tests	1	0.02	1333	46	11	274	259

2.3. Analytical techniques

The acid concentration of the samples collected along the experiments was determined by titration with 0.01 and 0.1 mol/L NaOH solutions, using an automatic titrator (Mettler Toledo Titrator T70). The metal composition was determined by Inductively Coupled Plasma Optical Emission Spectrometer (5100 ICP-OES, Agilent Technologies) and Mass Spectrometer (7800 ICP-MS, Agilent Technologies). Finally, the anionic composition was determined by Ion Chromatography (IC), using a Dionex ICS-1100 with the IONPAC® AS23 anion exchange column. A mixture of 4.5 mmol/L Na_2CO_3 and 0.8 mmol/L $NaHCO_3$ was used as mobile phase. The samples were filtered through 0.22 μm and diluted with Milli-Q water for IC and 2 % HNO_3 for ICP-OES/MS analysis.

2.4. Solution chemistry speciation

Transport of the different species in solution is largely influenced by their speciation. The speciation of the main solutes involved in the study in the synthetic solutions (see Figure S1) was performed by using PHREEQC [28] with the extended PITZER database reported by Vicari et al. [8]. In the pH range of the solutions used (highlighted with the green rectangles in Figure S1), several cases can be observed: (i) B and Ge are present as neutral species (H_3BO_3(aq) and H_4GeO_4(aq)); (ii) Ga is mostly present in its cationic form (Ga^{3+}) and forms complexes with chloride and sulphate at pH close to 1 ($GaCl^{2+}$, $GaSO_4^+$, $Ga(SO_4)_2^-$); and (iii) Co and Sr are mainly present in their cationic forms (Co^{2+} and Sr^{2+}), although there would be a minimum presence of their chloride and sulphate complexes ($CoCl^+$, $SrSO_4$(aq) and $SrCl^+$).

2.5. Modelling diffusion dialysis applications by coupling mass balances and transport equations

The mathematical model used in this work was adapted from Gueccia et al. [20] (HCl and $FeCl_2$ solutions) and Ruiz-Aguirre et al. [23]

(H_2SO_4 and $CuSO_4$ solutions).

The modelling approach is based on a 1D model that discretizes the module length along the two channels. The time variation of concentration and volume in the two solutions tanks were also considered. Table 2 collects the main equations used to describe ion and water flux across the AEM. The species flux across the membrane was described by a diffusive transport equation, which accounts for three mass-transfer resistances: (i) boundary layer on the feed side, (ii) membrane, and (iii) boundary layer on the recovered acid side. Therefore, the total species flux can be described as shown in Eq. (1), where the overall mass transfer coefficient (U_i) is defined in Eq. (2). In this case, the mass transfer coefficient in a laminar regime with forced convection in planar configuration is shown in Eq. (3). The Sherwood (Sh) refers to the boundary layer transport phenomena, and in this case, considering the geometry of the channel, the characteristic length is the thickness of the channel. With the values of bulk solution diffusion coefficients and the characteristic length, the Sh number allows to determine the mass transfer coefficients at both membrane sides ($k_{i,r}$ and $k_{i,d}$ for the feed and diffusate sides, respectively). Moreover, the water flux (Eq. (4)) is expressed as a combination of osmotic (related to the osmotic pressure difference across the AEM, Eq. (5)) and drag (related to the transport of solvated species, Eq. (6)) fluxes. In this case, the osmotic pressure was determined using the Van't Hoff equation. Solvation numbers adopted were 1 for H^+, 8 for SO_4^{2-} and 6 for Cl^-.

To close the model, global and components mass balance equations (1D differential) were adopted, in order to calculate the flow rate and concentration variation along the channel.

It should be highlighted that due to the low concentrations of the TEs (e.g., B, Ga, Ge, Co and Sr), their contribution to the water flux (i.e., osmotic pressure and solvation) as well as the salt effect were neglected to reduce the mathematical complexity of the model and allow a fast resolution time.

The mathematical model requires also to know the physical properties of solutions and species. The density correlations with concentrations were derived from Lalibertè et al. [29], whereas diffusion coefficients for bulk solution were taken from Vanýsek [30].

Initially, the model was used to describe and characterise the behaviour of the DD unit when using the batch configuration. In this case, an optimization algorithm implemented in Matlab® allowed to find the best fitting between model predictions and experimental data by determining the set of membrane permeabilities to species. It should be noted that membrane permeabilities, based on Solution-Diffusion model, account for the partition coefficients and the diffusion coefficients inside the membrane. Once the permeabilities were determined, the prediction capability of the mathematical model was validated with the once-through experiments.

2.6. Performance indicators

Different performance indicators were used to compare the data.

For the batch experiments, two different parameters were defined. The first one, the recovery (see Eq. (7.a)), accounts for the mass of one species that has been transported from the feed to the diffusate. It should be mentioned that, as the tests performed were under batch configuration, the equilibrium is limiting a 50 % recovery (i.e., equal concentrations at both sides). The second one is the ionic molar flux (see Eq. (7.b)).

$$Recovery(\%) = \frac{C_{i,d,t}\cdot V_{d,t}}{C_{i,f,0}\cdot V_{f,0}}\cdot 100\% \tag{7.a}$$

$$J_i\left(\frac{mol}{m^2\cdot h}\right) = -\frac{1}{A_{mem}}\cdot\frac{d\left(C_{i,f}\cdot V_f\right)}{dt} \tag{7.b}$$

where C is the molar concentration (mol/L), V is the volume of the compartment (L), A_{mem} is the membrane area (m^2) and t is the operating time (h). Subscript i refers to the species i, f and d to the feed and diffusate, respectively, t and 0 refer to a given operating time and to the beginning of the experiment.

For the once-through tests, data was plotted as function of the specific flow rate (see Eq. (8.a)), defined as the ratio between the flow rate and the total membrane area. Given the composition of the samples collected, the species transport (see Eq. (8.b)) was determined.

$$Specific\ flow\ rate\left(\frac{L}{m^2\cdot h}\right) = \frac{Q}{A_{mem,TOT}} \tag{8.a}$$

$$Species\ transport(\%) = \frac{Q_{dif}\cdot C_{dif}}{Q_{dia}\cdot C_{dia} + Q_{dif}\cdot C_{dif}}\cdot 100\% \tag{8.b}$$

where Q is the flow rate (L/h), $A_{mem,TOT}$ is the total membrane area (m^2), and C is the molar concentration (mol/L). Subscripts dif and dia refer to the diffusate and dialysate.

3. Results and discussion

3.1. Characterization of species' transport in acidic solutions by using batch mode diffusion dialysis tests

3.1.1. Transport of hydrochloric acid

Fig. 2 shows the concentration profiles for HCl, obtained with the tests performed with pure HCl solutions at different initial concentrations (Experiments #1–4), as a function of the operating time for both the feed and diffusate solutions. Symbols represent the experimental

Table 2
Main equations used to describe ion and water transport across the anion exchange membrane.

Species flux across the anion exchange membrane	
$J_i = U_i\cdot\Delta C_i = U_i\cdot(C_{i,r} - C_{i,d})$	(1)
$U_i = \left[\frac{1}{k_{i,r}} + \frac{1}{P_i} + \frac{1}{k_{i,d}}\right]^{-1}$	(2)
$Sh = \left(-1.481\cdot10^{-7}Re^5 + 3.739\cdot10^{-5}Re^4 - 0.003253Re^3 + 0.1118Re^2 + 0.1348Re + 6.9536\right)\left(\frac{Sc}{600}\right)^{0.5}$	(3)
Water flux across the anion exchange membrane	
$J_w = J_{os} + J_{dr}$	(4)
$J_{os} = P_w\cdot(\pi_r - \pi_d)$	(5)
$J_{dr} = \sum_i \beta_i\cdot J_i$	(6)

Where J_i is the species flux across the AEM (mol/(m^2·s)), U_i is the overall mass transfer coefficient (m/s), $C_{i,r}$ and $C_{i,d}$ are the molar concentrations at the feed and diffusate side (mol/m^3), respectively, $k_{i,r}$ and $k_{i,d}$ are the mass transfer resistances at the feed and diffusate side (m/s), respectively, P_i is the membrane permeability to the species i (m/s), J_w, J_{os} and J_{dr} are the total, osmotic and drag fluxes across the AEM (L/(m^2·s)), P_w is the hydraulic membrane permeability (L/(m^2·s·bar)), π is the osmotic pressure (bar) and β_i is the solvation number of species i.

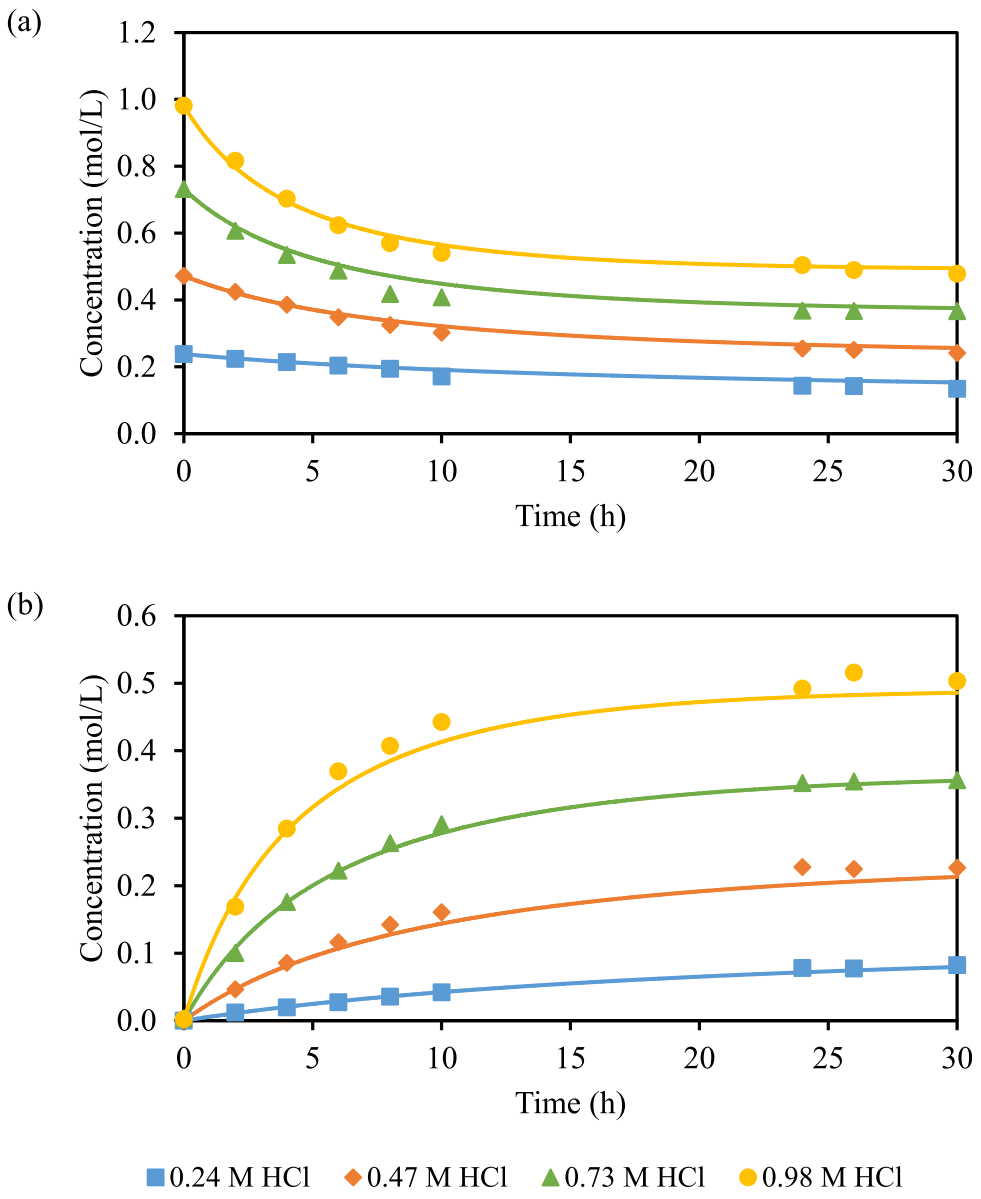

Fig. 2. Concentration profiles of HCl in the (a) feed and (b) diffusate as a function of time and initial acid concentration in the experiments #1–4. Specific flow rate: 709 L/(m^2·h). Symbols: experimental data, lines: model fitting.

data, whereas lines show the model fitting.

It can be observed that the concentration profiles on the feed side followed a similar trend (see Fig. 2.a). The concentration of HCl started to decrease, reaching an asymptote after 24 h, which approximately represents half of the initial concentration. It can also be noticed that the acid flux was higher when the initial concentration increased, which was mainly related to a higher concentration gradient between both membrane sides (see Figure S2). Similarly, the acid concentration started to increase on the diffusate side (Fig. 2.b), reaching a similar plateau after 20 h, where the concentration gradient across the membrane has been completely depleted (thus leading to null flux). While the acid recovery at the end of the experiment was 32 % for the tests at lower HCl concentration, 45–50 % was achieved in the rest of the tests, which is near the maximum recovery that could be attained (i.e., 50 %) in batch experiments with equal feeds volumes. This good performance was expected since the membrane used (i.e., AEM), containing quaternary ammonium functional groups (e.g., –NR_3^+, positively charged), allows the transport of Cl^- ions as postulated by the Donnan exclusion phenomena [31]. However, a stoichiometric amount of cations must permeate in order to keep the electroneutrality condition at the diffusate side. Therefore, and because of its small size, H^+ also moved. Similar results were obtained by Palatý and Bendová [32], who studied the transport of inorganic acids across a Fumasep FAD membrane at different concentration levels in batch configuration. Similar to the present work, the authors reported a faster transport of HCl across the membrane when increasing the concentration.

Figure S3 collects the volume variation in both compartments as function of time and the initial HCl concentration. It can be observed that the volume of the feed solution increased along the operating time, and such increase was higher in more diluted solutions. The volume variation was related to the water flux caused by a combination of (i) osmosis, where water flowed from the diluted to the concentrated compartment (from the water to the feed side), and (ii) drag flux, related to the transport of solvated ions from the feed side to the water side. In all scenarios, osmosis prevailed over the drag flux, explaining why higher volume was collected in the feed side, but as acid concentration increased the net flux of water from the water to the feed side became lower, resulting in smaller volume variation at large concentrations.

The operating time was shortened to 10 h for the following experiments. In this case, as batch tests were performed with equal feed volumes, the equilibrium is attained at 50 % acid recovery. Considering that after 10 h test, around 80 % of equilibrium was already attained, the tests were shortened.

3.1.2. *Transport of sulphuric acid in hydrochloric acid media*

The variation in concentration of H_2SO_4 was investigated in experiments #5–7, where different initial concentrations of sulfuric acid were added to a 1 mol/L HCl solution. Concentration profiles are shown in Fig. 3 as a function of time for both the feed and diffusate.

Similar to the previous case, the concentration of H_2SO_4 in the feed profiles (Fig. 3.a) decreased along the experiment, causing an increase of its concentration in the diffusate side (Fig. 3.b). Unlike the HCl final concentration on the feed side for these tests, which was about half of the initial, (see Figure S4), the final H_2SO_4 concentration represented around 65 % of the initial one. Thus, at the end of the experiments, around 41 % of the HCl was recovered (similar recovery was found at 10 h during the single HCl tests), whereas the recovered H_2SO_4 was lower (30–37 %). This difference in the performance was mainly related to the ionic size of both transported acid anions (e.g., Cl^- and HSO_4^-), resulting in a physical impediment for the biggest ones (i.e., the ones from H_2SO_4) to pass through the membrane. As it was also previously seen, the higher the driving force of the DD process (i.e., the concentration gradient between feed and diffusate), the higher the sulphuric acid flux (see Figure S5). Moreover, the concentration of H_2SO_4 did not affect the flux

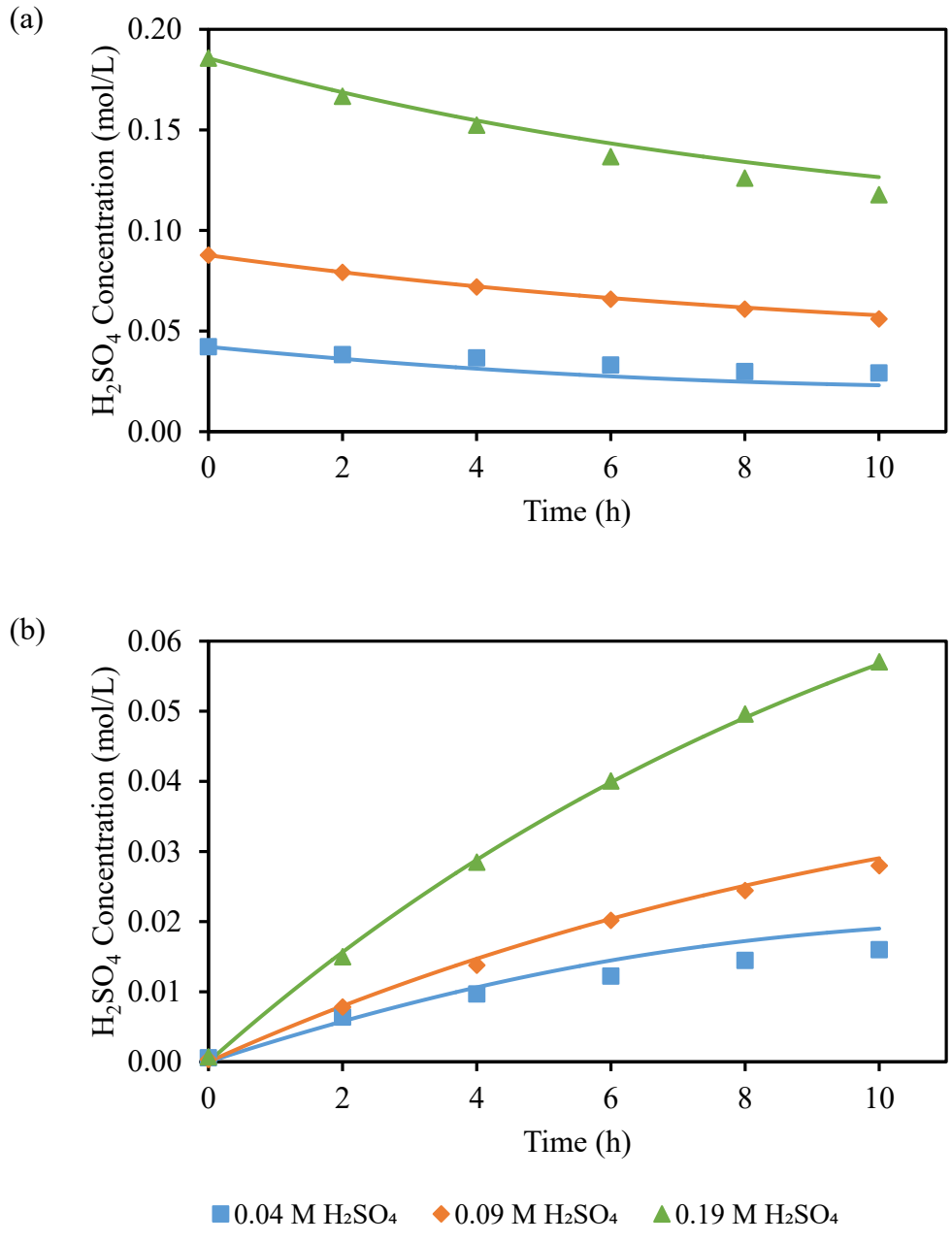

Fig. 3. Concentration profiles of H_2SO_4 in the (a) feed and (b) diffusate as a function of time and initial sulphuric acid concentration (in the presence of 1 mol/L HCl) in the experiments #5–7. Specific flow rate: 709 L/(m^2·h). Symbols: experimental data, lines: model fitting.

of HCl. Similarly to the previous case, an increase on the volume of the feed solution was noticed (see Figure S6), which was related to a higher osmotic flux over the drag one. However, as acid concentration increased, the increment of feed volume was lower.

H_2SO_4 is present as totally dissociated species HSO_4^- and H^+. Therefore, the good performance observed was related to the fact that the oxyanion is transported thanks to the quaternary ammonium groups of the AEM, and H^+ are co-transported to maintain the electroneutrality.

3.1.3. Transport of weak oxoacids (boron, gallium and germanium) in hydrochloric and sulphuric acid media

Along the TEs present in the bitterns, B, Ga and Ge appear as weak oxoacids or oxyanions species (H_3BO_3, $Ga(OH)_3$(aq) and H_4GeO_4(aq)), as it could be seen in Figure S1. However, it should be mentioned that in the typical solutions generated in the regeneration of IX sorbents (i.e., concentrated HCl or H_2SO_4 solutions) B and Ge are present as neutral oxoacid forms, while Ga is mainly present as cationic form, as shown in Figure S1. Therefore, their concentration profiles obtained in tests #8–10, starting with different initial concentrations, are shown in Fig. 4 as a function of time for both the feed and diffusate sides.

Despite having different initial concentrations, a clear decrease can be observed for B and Ge on the feed side. Nevertheless, the decrease is not as sharp as the ones previously shown for HCl and H_2SO_4, which may be related to the fact that these two oxoacids, in acidic media, remain as neutral species (H_3BO_3(aq) and H_4GeO_4(aq)). Therefore, their transport could not be associated to the main mechanism of Cl^- (for HCl) and HSO_4^- (for H_2SO_4), which is based on an electric attraction between the anions and the positively charged quaternary ammonium groups of the AEMs. Considering that both species are neutral, their transport can be associated to a weaker mechanism driven by diffusion, where the neutral species are diffused through the pore volume of the polymer matrix of the AEM. As a result of this weaker mechanism, the rejections obtained for both B and Ge were around 82 %. In addition, no Ga transport was observed from the feed to the diffusate side. Although Ga is found as oxyanion in the bittern, it converts to a cation form (Ga^{3+}) in acidic media (see Figure S1) and, therefore, its transport through the AEM is totally hindered and, then, it remains in the feed side. Rejection values exceeding 96 % were obtained for Ga in all experiments #8–10, and this low transport ratio is due to the need to compensate the charge of the anions transported (e.g., Cl^- and HSO_4^-).

Similar conclusions were achieved by López et al. [24] when treating an effluent from the off-gases treatment from Cu smelters (220 g/L H_2SO_4, 3.4 g/L As(III,V)). The presence of As as either As(III) or As(V) in acidic media resulted in their presence as neutral species (e.g., H_3AsO_4 for As(V) or H_3AsO_3 for As(III)). Both of them were partially transported (ca. 40–50 %) across the membrane with the similar mechanism postulated for the B and Ge species.

3.1.4. Transport of cationic species (cobalt and strontium) in hydrochloric and sulphuric acid media

Fig. 5 shows Co and Sr concentration profiles in tests #11–13, starting with different initial concentrations, as a function of time for both the feed and diffusate sides. As it is described in Figure S1, Co(II) and Sr(II) are present as cationic species (Co^{2+} and $CoCl^+$ for Co(II) and Sr^{2+} for Sr(II)) both in the bittern and the acidic media used in the experiments. Therefore, the positively charged AEM completely rejected them (>97 %) according to Donnan exclusion. Limited transport was observed from the feed to the diffusate based on a diffusive transport. In fact, although a slight increase can be observed in the diffusate graphs, regarding their concentration's order of magnitude (i.e., 10^{-6} mol/L), it can be considered almost negligible. The transport of co-ions across IX membranes is related to the Donnan potential, i.e., the electric potential that arises at the membrane-solution interface. The exclusion of co-ions can be related to the large fixed charge density, which in turn results in a small sorption in the membrane phase, but also to the low concentration in the external electrolyte [33].

The removal of metallic impurities from acid has been widely studied in the literature. For instance, Luo et al. [34] evaluated the presence of metal ions (Fe^{2+}, Ni^{2+}, Cu^{2+}, Zn^{2+}, Al^{3+}) in HCl solutions. The authors reported the importance of solution speciation, especially when working in HCl media, since metals can form cationic ($FeCl^+$, $NiCl^+$, $CuCl^+$) or anionic complexes ($ZnCl_3^-$). Depending on their presence, the membrane

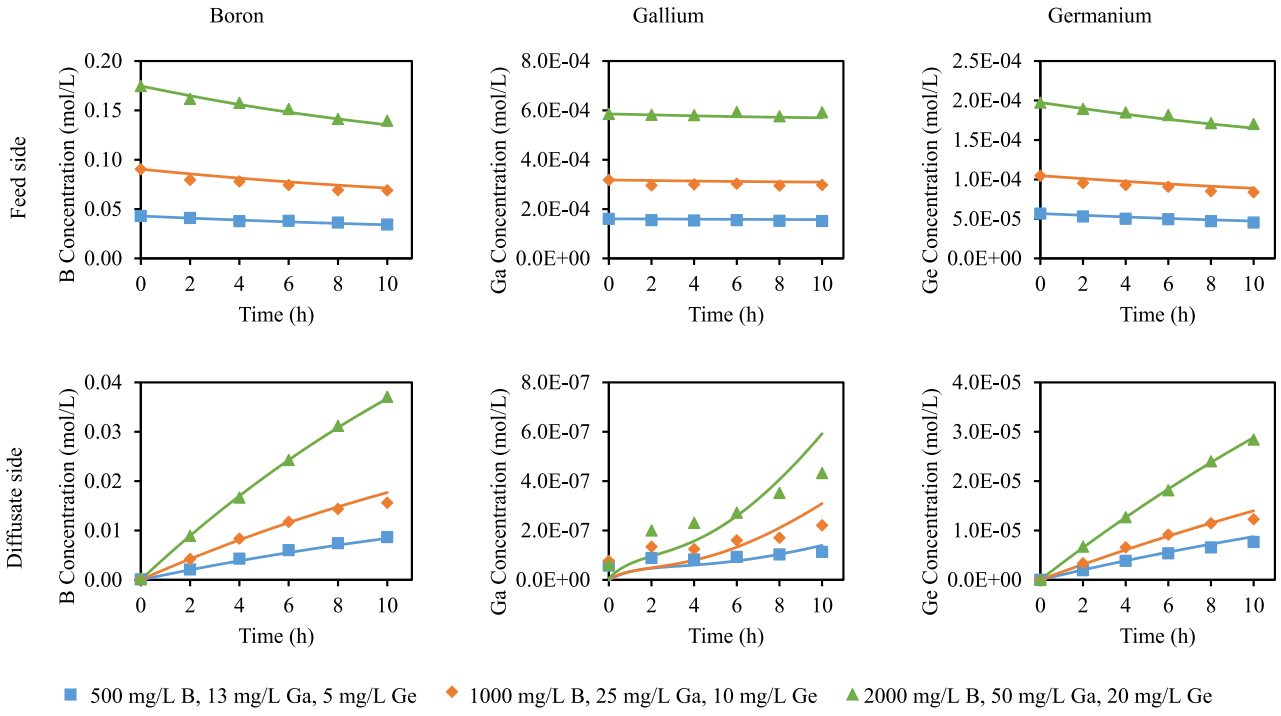

Fig. 4. Concentration profiles of B, Ga and Ge in the feed and diffusate as a function of time and initial concentration (in the presence of 1 mol/L HCl and 0.1 mol/L H_2SO_4) in the experiments #8–10. Specific flow rate: 709 L/(m^2·h). Symbols: experimental data, lines: model fitting.

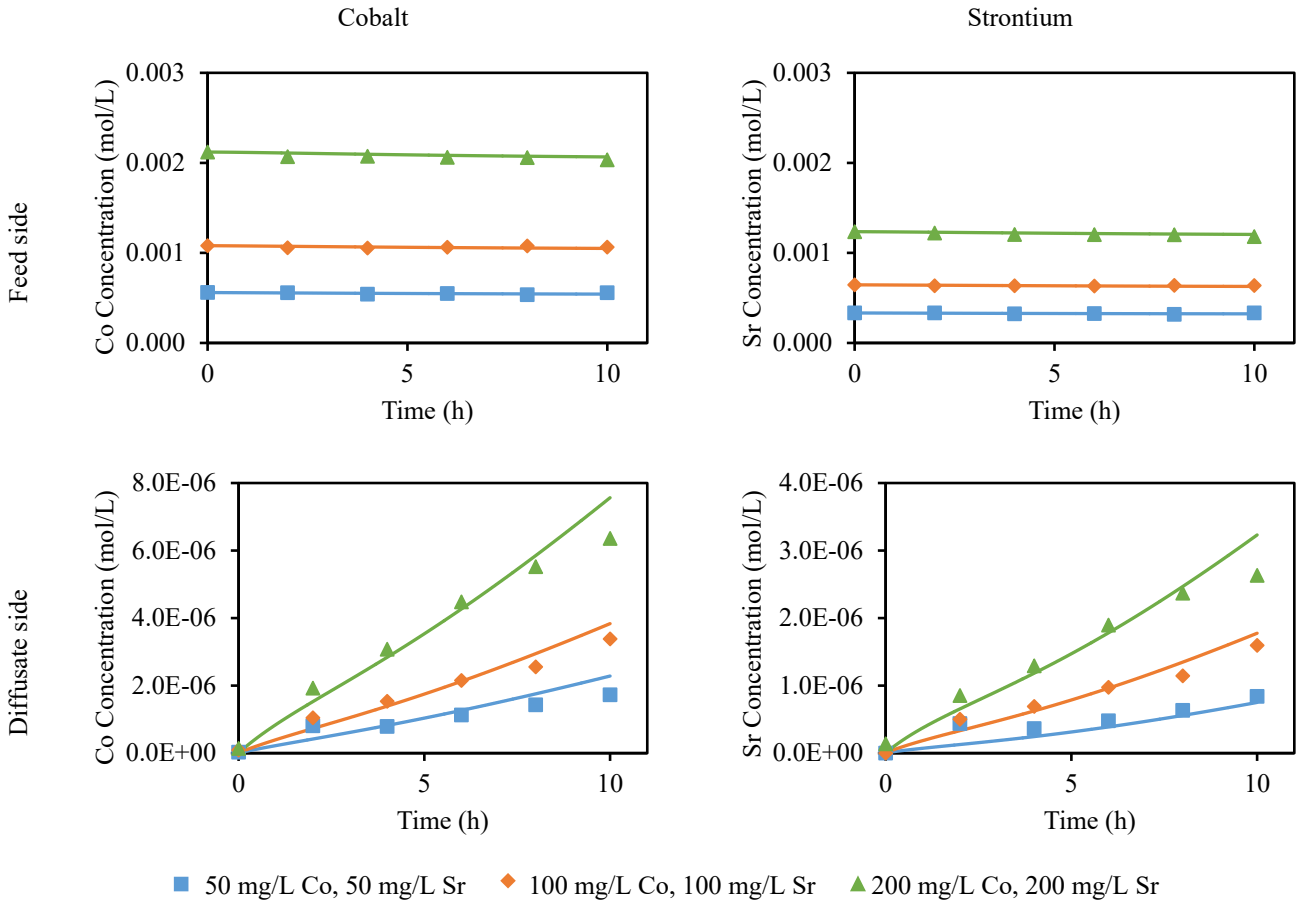

Fig. 5. Concentration profiles of Co and Sr in the feed and diffusate as a function of time and initial concentration (in the presence of 1 mol/L HCl and 0.1 mol/L H_2SO_4) in the experiments #11–13. Specific flow rate: 709 L/(m^2·h). Symbols: experimental data, lines: model fitting.

was able to reject cationic ones, whereas anionic ones permeated across the membrane. Palatý and Žáková [35] studied the transport of HCl and $ZnCl_2$ mixtures across the Neosepta-AFN membrane. At high $ZnCl_2$ concentrations (e.g., >0.5 mol/L), higher HCl concentrations were achieved in the diffusate than in the dialysate due to the salt effect (the presence of salts containing the same anion as the acid enhances the H^+ diffusion through the membrane [36]). It should be mentioned that, in the data shown in the present work, such effect was not observed due to the low metal concentration (in the order of mmol/L). Apart from that, the presence of Zn(II) in the diffusate due to its presence as anion (e.g., $ZnCl_3$) was also measured. Palatý et al. [37] also reported the salt effect when working with HCl and $FeCl_3$ mixtures, but in this case, the iron transport remained below 8 % due to the presence of Fe(III) as $FeCl^{2+}$, which was excluded by the membrane functional groups charge. In a similar study, Gueccia et al. [20] reported a leakage of Fe below 7 % working with HCl and $FeCl_2$ mixtures where Fe(II) was present as $FeCl^+$.

3.1.5. Species transport characterization by means of membrane permeabilities (P_i)

Given the experimental concentration profiles, the model was calibrated by optimising the set of permeability values that could describe accurately the observed trends by an optimization algorithm implemented on Matlab®. As can be observed, the model provided an accurate description of the experimental trends, being able to capture the concentration profiles in both feed and diffusate sides (see lines in Fig. 3-Fig. 5). Both obtained values and correlations for specific permeabilities as a function of feed concentration, are shown and commented in the following paragraphs. It should be highlighted that based on the definition of membrane permeability, it includes the diffusion coefficient in the membrane, which is expected to be from one to three orders of magnitude lower than that of the bulk solution [33].

Fig. 6 shows the membrane permeabilities towards HCl and H_2SO_4 as a function of their initial concentration. It should be mentioned that based on Donnan's derivation, the selectivity of AEMs for counter-ions is normally high when the external electrolyte concentration is smaller than the fixed charge concentration of functional groups in the membrane [33]. For HCl, a linear dependence of the membrane permeability with concentration was observed, whereas for H_2SO_4, such dependency was inversely proportional. This behaviour has already been described [23,32], and it could be related to the H_2SO_4 properties, as an increase in the acid concentration can cause a higher viscosity, then hindering the transport of acid across the membrane [32]. Moreover, it can be related to a decrease in membrane swelling and, therefore, with a membrane dehydration, which can cause a frictional resistance for acid permeation [36]. In addition, the interactions between the counter-ions and fixed ionic groups are influenced by the coulombic forces and hydration effect of the ions [33]. Apart from that, a decrease in both adsorption and permeability of sulphates was noticed when increasing H_2SO_4 concentration [38,39]. Contrary, the permeability for HCl is directly proportional to its concentration, which is related to a higher ionic mobility and diffusivity inside the membrane [40].

As a result, Eqs. (9) and (10) were derived to express the dependence of membrane permeabilities on initial concentration, which were used to fit the experimental data. The permeability towards HCl (Eq. (9)) shows a direct linear dependence, whereas, for H_2SO_4, the permeability is inversely proportional to the acid concentration (Eq. (10)).

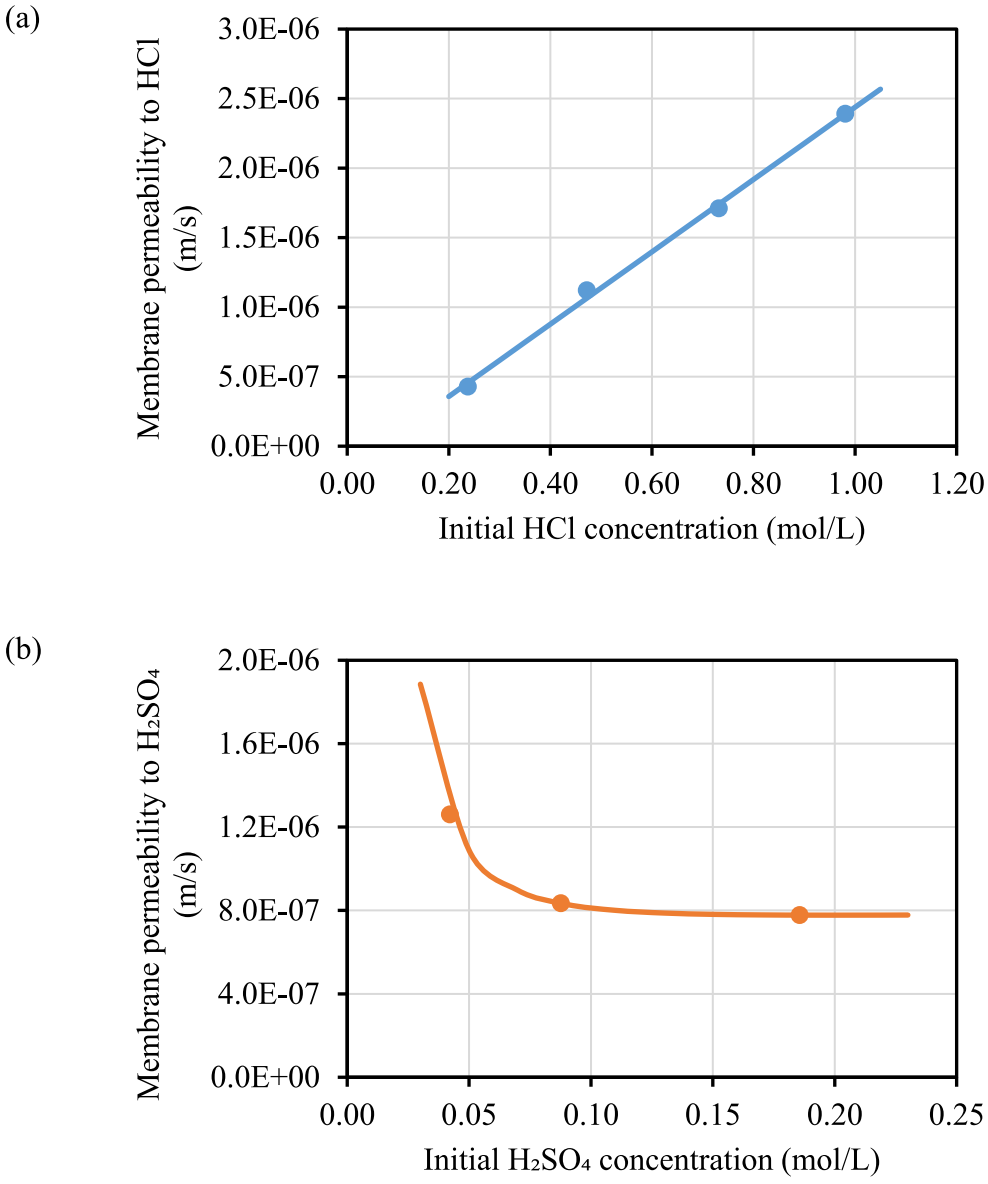

Fig. 6. Fitting of membrane permeability (P_i) to (a) HCl and (b) H_2SO_4 as a function of initial concentration.

$$P_{HCl}\left(\frac{m}{s}\right) = 2.6{\cdot}10^{-6}{\cdot}C_{HCl}\left(\frac{mol}{L}\right) - 1.63{\cdot}10^{-6} \quad (9)$$

$$P_{H_2SO_4}\left(\frac{m}{s}\right) = 1.38{\cdot}10^{-9}{\cdot}\left(\frac{1}{C_{H_2SO_4}\left(\frac{mol}{L}\right)}\right)^2 - \frac{1.38{\cdot}10^{-8}}{C_{H_2SO_4}\left(\frac{mol}{L}\right)} + 8.12{\cdot}10^{-7} \quad (10)$$

Such values are similar to the ones reported by Palatý and Bendová [32], ranging from $0.37{\cdot}10^{-5}$ to $1.34{\cdot}10^{-5}$ m/s for HCl and from $4.40{\cdot}10^{-5}$ to $1.02{\cdot}10^{-5}$ m/s for H_2SO_4 when the concentration was increased from 0.2 to 2 mol/L. Moreover, the authors reported an increasing dependence on permeabilities for HCl on concentration, whereas for H_2SO_4 it was inversely proportional. Similarly, Luo et al. [41] reported membrane permeability values for HCl and H_2SO_4 of $1.60{\cdot}10^{-6}$ m/s in 1.2 mol/L HCl + 0.6 mol/L NaCl and $2.5{\cdot}10^{-6}$ m/s in 0.6 mol/L H_2SO_4 + 0.3 mol/L Na_2SO_4. Under the same conditions of acidity, they reported membrane permeability values of $1.40{\cdot}10^{-6}$ m/s for HCl (in $FeCl_2$ solutions) [42].

Similarly, Fig. 7 shows the membrane permeabilities towards the TEs for the six experiments carried out. Different trends could be observed: (i) in the case of oxoacids, the fact that both B(III) and Ge(IV) were present as neutral species at acidic pH values allowed their transport across the membrane through de diffusion based mechanism; (ii) the case of Ga(III), present in a cationic form (i.e., Ga^{3+}), which is excluded by the positively charged membrane; and (iii) the case of Co(II) and Sr (II) in cationic forms, which are also excluded by the membrane. Due to the positive species for Ga, Co and Sr, the membrane showed permeabilities two orders of magnitude lower than those of B and Ge.

Based on the obtained values, the AEM exhibits a high selectivity towards the acid, following the order: HCl > H_2SO_4 > B > Ge ≫ Co > Sr > Ga. The selectivity in IX membranes is defined by the nature of the membrane itself (nature of the polymer, pore structure, charge of the membrane's functional groups, thickness and charge density) and the solution composition and properties (ionic strength, viscosity, temperature and presence of competitive ions) [33]. In order to tune the membrane properties, current practices involve surface modification by layer-by-layer techniques to make AEMs more selective towards Cl^-

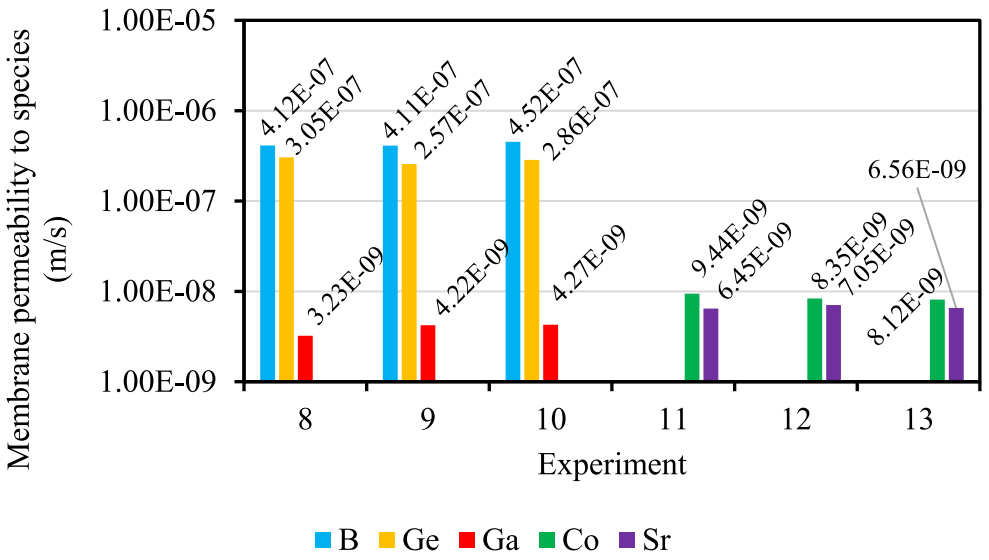

Fig. 7. Membrane permeabilities (P_i) to TEs in acidic solutions containing 1 mol/L HCl and 0.1 mol/L H_2SO_4 at different initial TEs concentrations for experiments #8–13 (see Table 1).

rather than SO_4^{2-} [43,44], or by depositing a dense neutral layer on the AEM to increase the monovalent selectivity [45].

3.2. *Once-through tests: Effect of specific flow rate and flow rate ratio on acid recovery and species passage*

When operating with the once-through configuration, the influence of specific flow rates on acid recovery and species transport was firstly evaluated, keeping the same flow rate for both acid and water. Experiments were performed with a multi-ionic solution (see Table 1), and data is represented in Fig. 8, where the right graphs present a zoomed section of the graph with trends of the species less transported, in a larger scale. Experimental data is represented with symbols, whereas the model prediction (using the above determined membrane permeabilities) is plotted as continuous lines.

It can be observed that the highest acid recovery was attained at the

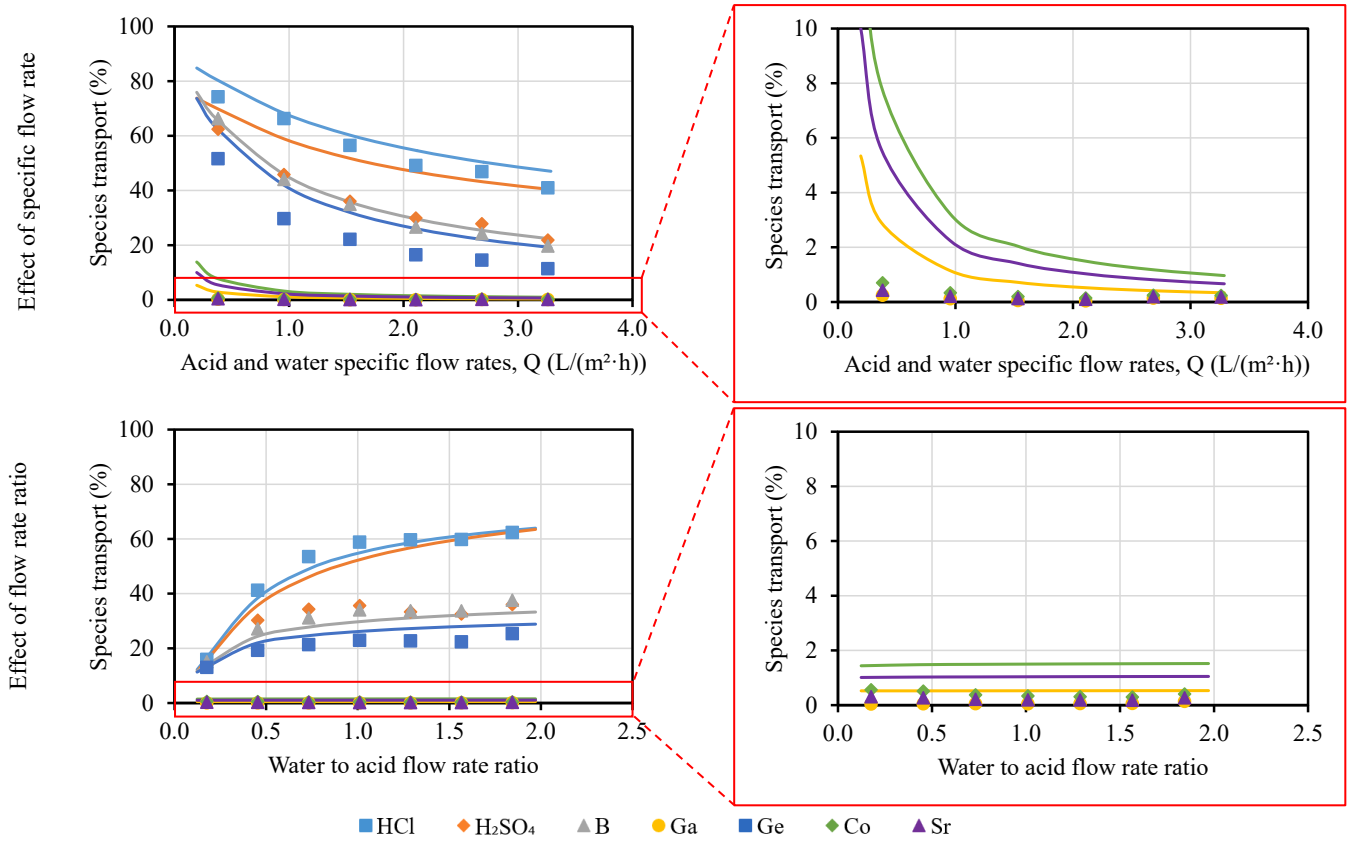

Fig. 8. Effect of specific flow rate and flow rate ratio (at 2.11 L/(m^2·h) acid specific flow rate) on species transport in the once-through experiments. Symbols: experimental data. Lines: model prediction. The right graphs present the species less transported in a larger scale.

lowest specific flow rate evaluated (74 % HCl and 62 % H_2SO_4). As both specific flow rates increased, acid recovery decreased to values of 41 % HCl and 22 % H_2SO_4 when reaching 3.26 L/(m^2·h), likely due to the much lower residence time, passing from 18.8 to 1.1 min (considering a volume inside the stack of 0.33 L), notwithstanding the increased species flux obtained thanks to the larger concentration driving force (see Fig. 9). In fact, working at low specific flow rates, the diffusate (or water side) got quickly saturated, which reduced the concentration gradient between both sides of the membrane and, therefore, the acid flux (see Figure S7.a). In turn, higher specific flow rates promoted a large concentration gradient which favoured the ionic flux.

With respect to the TEs, two different behaviours can be observed: one referring to oxoacids (e.g., B, Ge) group and the other related to cationic species (e.g., Sr, Co, Ga). In the first case, both oxoacids were easily transported across the membrane, but to a lesser extent than the acid. As an example, B was transported around 66 % at 0.38 L/(m^2·h) and such value decreased to 20 % at 3.26 L/(m^2·h). Similarly, Ge presented lower recoveries, moving from 52 % at 0.38 L/(m^2·h) to 11 % at 3.26 L/(m^2·h). As stated before, both species are present as neutral species (H_3BO_3(aq) and H_4GeO_4(aq)), thus the exclusion is based on steric hindrance. Conversely, the cationic species (i.e., Ga^{3+}, Sr^{2+}, Co^{2+}/$CoCl^+$) were rejected by the positively-charged membrane in agreement with Donnan exclusion [31], which limited their transport to values below 1 % in all the evaluated ranges.

Considering that the objective was to recover the maximum amount of acid with the lowest losses of TEs, it was decided to take a compromise solution. Therefore, the acid specific flow rate was fixed at 2.11 L/(m^2·h) for the subsequent tests. Under these conditions, it was possible to recover 49 % HCl and 30 % H_2SO_4, with losses of 27 % B, and 17 % Ge, whereas metal cations losses remained below 1 %.

Fig. 8 also collects the effect of the flow rate ratio on the species transport across the membrane. As mentioned before, the specific flow rate of acid was fixed at 2.11 L/(m^2·h), and the one for water was varied.

In this case, HCl recovery increased from 16 % at a water to acid flow rate ratio of 0.18 to 62 % at a ratio of 1.84. A similar behaviour was noticed for H_2SO_4, moving from 13 % to 36 % within the same flow rate ratio. This tendency was related to the fact that the acid flow rate was too high in comparison to the one of water at the lowest flow rate ratio values. Therefore, the concentration of acid in the diffusate increased rapidly thus leading to a much smaller driving force across the membrane, and therefore to lower acid fluxes (see Fig. 9), not enough to guarantee the expected recoveries. As depicted in Figure S7.b, the diffusate reached the same concentration as the dialysate within the stack when working at low water to acid flow rate ratios. However, when working at high ratios, a high concentration gradient was maintained along the stack, which favoured the ionic flux across the membrane. Similar transport profiles were obtained for the non-charged TEs in the solution, as they followed the order B (around 34 %) > Ge (around 23 %). In the case of Co, Sr, and Ga their transport remained below 1 %. Moreover, a plateau in recoveries was observed at flow rate ratios higher than 1. This phenomenon was related to the fact that the limiting factor is not the driving force anymore, but the main resistance for species transport across the membrane and the reduced permeability, which was not affected significantly by the flow rate variation. A maximum flux in DD could be related to the case where the water has no ions in solution along the treatment, which takes place at infinite water flow rate. Under these conditions, the mathematical model allowed to estimate those values, which turned to be 1.64 mol/(m^2·h) for HCl, 0.33 mol/(m^2·h) for H_2SO_4, and 0.11 mol/(m^2·h) for B, whereas in the case of TEs, they followed the order: Co (0.14 mmol/(m^2·h)) > Ge (0.10 mmol/(m^2·h)) > Sr (0.07 mmol/(m^2·h)) > Ga ($7.1 \cdot 10^{-3}$ mmol/(m^2·h)).

When Xu et al. [21] evaluated HCl recovery from a waste solution (3 mol/L HCl, 2.7 mol/L Fe, 0.07 mol/L Zn) under once-through mode, HCl recoveries higher than 88 % HCl at a flow rate ratio within the range

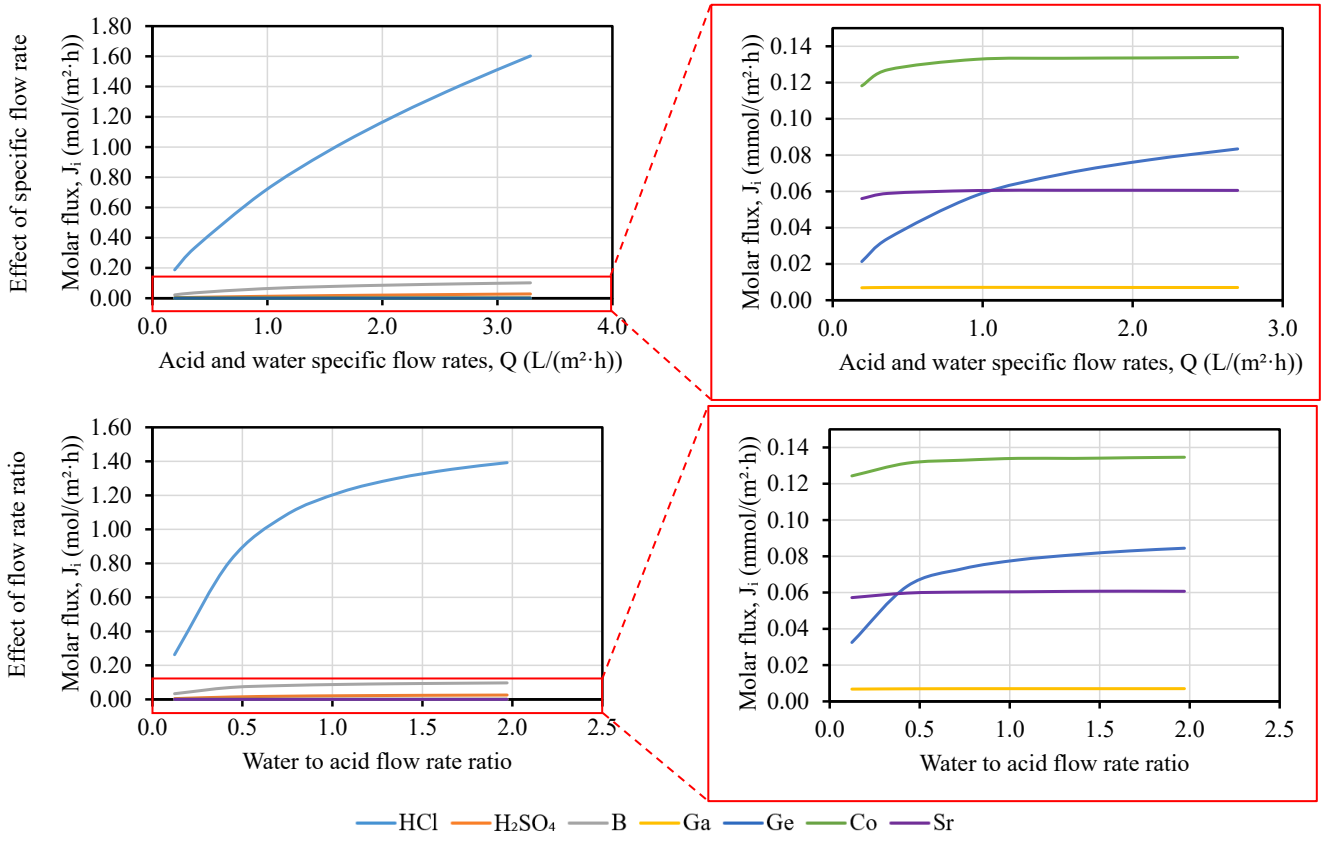

Fig. 9. Effect of specific flow rate and flow rate ratio (at 2.11 L/(m^2·h) acid specific flow rate) on fluxes in the once-through experiments. Lines: model prediction. The right graphs present the species less transported in a larger scale.

2–3.2 (0.42 L/h acid flow rate) were achieved. With regard to metals, Fe leakage moved from 11 to 23 %, whereas the one of Zn was higher than 56 %. López et al. [24] were able to recover more than 70 % of H_2SO_4 at the optimum conditions (specific flow rates equal to 0.86 L/(m^2·h)). However, the authors observed an As transport of around 39 % working in once-through mode due to its presence as a neutral species, whereas metals were rejected by more than 85 %. Bendová et al. [46] studied acid transport in 3 mol/L HCl and 0.5 mol/L $FeCl_3$ mixtures in once-through mode with different commercial membranes. Acid recoveries around 89 % for AFN and 92 % for FAD membranes at 0.1 L/h were achieved. However, these values decreased to 75 % and 80 % for AFN and FAD, respectively, at 0.2 L/h. Under the range studied, Fe^{3+} transport was below 14 % for FAD and below 16 % for AFN. Gueccia et al. [47] integrated DD, membrane distillation and crystallization at pilot plant scale to valorise industrial pickling solutions. Recoveries around 82 % HCl were achieved, whereas the Fe(II) and Zn(II) transport was 40 % and 53 %, respectively, due to the formation of Zn-complexes with chlorides.

About the model performance, Eqs. (9) and (10) were used to predict the HCl and H_2SO_4 fluxes across the membrane, whereas for TEs the lowest membrane permeability was used to carry out the simulations. It can be observed that the model predicted the experimental trends in most of the cases (see Figure S8 and continuous lines in Fig. 8). For both types of experiments, the model properly captured the trends for HCl and B. In addition, small deviations were observed for the TEs (Ge, Ga, Co and Sr). In fact, the model predicted a slightly higher transport of these compounds across the membrane than the ones obtained experimentally, which can be related to an overestimation of the membrane permeabilities showed in Fig. 7. Therefore, lower membrane permeabilities could be able to predict properly their experimental trends. However, bigger differences were observed for H_2SO_4, which can be related to a shift of equilibrium of the second acid dissociation (HSO_4^-/SO_4^{2-}) towards SO_4^{2-} as the acid was being removed. This species was not considered in the model, and it would be expected to suffer a higher exclusion from the membrane. Moreover, the model failed to predict the experimental trends at the lowest specific flow rate for all the elements, which was related to the correlations used to describe the transport in the boundary layers.

Overall, the results highlighted the possibility of recovering up to 59 % HCl and 36 % H_2SO_4 under the optimum conditions (acid specific flow rate of 2.11 L/(m^2·h), water to acid flow rate ratio of 1) with losses of 34 % and 23 % for B and Ge, respectively. In contrast, losses for cationic elements (i.e., Co, Ga, Sr) remained below 1 %. Considering the scenario where DD is applied prior to any crystallization process, the results would allow to fractionate the TEs. For instance, given the experimental data, both B and Ge could be easily recovered along with the acid and separated from the other TEs. For example, B could be recovered as H_3BO_3(s) via an evaporative crystallization [17], and Ge as a salt using tannic acid [48].

4. Conclusions

The current research assessed the performance of DD using the AEM Fumasep FAD-PET-75 for acid recovery from an eluate of IX resins, focusing on the migration of TEs intended to be recovered in subsequent stages.

Batch tests conducted on a single membrane sheet showed high recoveries of HCl (45–50 %) and H_2SO_4 (30–37 %), close to the maximum achievable in these batch experiments (50 %). Different behaviours were noted for targeted metals: neutral species such as B (H_3BO_3) and Ge (H_4GeO_4) permeated partially the membrane with 82 % rejection, whereas cations like Ga^{3+}, Co^{2+}, and Sr^{2+} were completely rejected (>96 %). Using a 1D transfer model, membrane permeability to these metals was inferred, providing values in the following order: Ga < Sr < Co ≪ Ge < B. Cations exhibited two orders of magnitude lower permeability (10^{-9} m/s) compared to neutral species (10^{-7} m/s), attributed to their charge and size. Permeability to HCl showed a linear dependence on its initial concentration, while for H_2SO_4, it was inversely proportional.

In once-through tests using an 8-membranes stack with simulated IX eluate, low specific flow rates (0.38 L/(m^2·h)) led to higher recovery (though lower species fluxes) across the membrane for acids (74 % HCl, 62 % H_2SO_4) and oxoacids (66 % H_3BO_3, 52 % H_4GeO_4) compared to a high specific flow rate (3.26 L/(m^2·h)) (41 % HCl, 22 % H_2SO_4, 20 % H_3BO_3 and 11 % H_4GeO_4). This difference was attributed to the longer residence time for the feed solution to interact with the membrane and water. Cationic metals (Ga^{3+}, Co^{2+}, Sr^{2+}) showed minimal transport (<1%) regardless of flow rate. Considering the results, a specific flow rate of 2.11 L/(m^2·h) was set for acid to further study the optimal flow rate ratio between acid and water.

Changing the water to acid flow rate ratios above 1 did not strongly affect the transport of the species (around 60 % HCl, 34 % H_2SO_4, 35 % H_3BO_3 and 23 % H_4GeO_4). On the contrary, reducing that ratio to lower values (up to 0.18) resulted in low migration of the studied species (16 % HCl, 14 % H_2SO_4, 15 % H_3BO_3 and 13 % H_4GeO_4) due to an excessively fast acid flow rate compared to water, causing the fast saturation of the diffusate and the low driving force. As in the previous case, cations transport (<1%) was not affected by the water to acid flow rate ratio. Excluding the lowest specific flow rate, the model successfully predicted the trends of all the species studied, especially those of HCl and B. However, it slightly overestimated the other TEs transport across the membrane, suggesting a lower membrane permeability than the one determined with batch tests.

The solution used in this study simulated the one obtained after recovering B, Co, Ga, Ge and Sr, all of them considered CRMs for the EU, from bitterns by applying sorption–desorption process in IX columns. As desorption was carried out with acids, the need to recover the excess of acid was essential to enhance circularity and promote resource recovery. Furthermore, it also allows a lower chemical consumption in subsequent steps to precipitate the desired minerals needed in the EU. The findings of the current research highlight that DD, specially known for being a cost-effective technology, allowed to effectively recover most of the acid from the IX column's eluate without a crucial loss of the targeted metals, aiding the EU to find an alternative source for CRMs.

CRediT authorship contribution statement

V. Vallès: Writing – original draft, Validation, Methodology, Investigation, Formal analysis, Data curation. **M. Fernández de Labastida:** Writing – review & editing, Validation, Methodology, Investigation, Formal analysis, Data curation. **S. Randazzo:** Writing – review & editing, Validation, Methodology. **A. Cipollina:** Writing – review & editing, Validation, Project administration, Methodology, Funding acquisition. **D. Winter:** Writing – review & editing, Validation, Methodology. **J. Koschikowski:** Writing – review & editing, Validation, Methodology. **J. López:** Writing – original draft, Validation, Supervision, Methodology, Investigation, Formal analysis, Data curation, Conceptualization. **J.L. Cortina:** Writing – review & editing, Validation, Supervision, Resources, Project administration, Methodology, Funding acquisition, Conceptualization.

Declaration of competing interest

The authors declare that they have no known competing financial interests or personal relationships that could have appeared to influence the work reported in this paper.

Data availability

The data will be available in Zenodo

Acknowledgements

This work was supported by the EU within SEArcularMINE (Circular Processing of Seawater Brines from Saltworks for Recovery of Valuable Raw Materials) project – Horizon 2020 programme, Grant Agreement No. 869467. This output reflects only the authors' view. The European Health and Digital Executive Agency (HaDEA) and the European Commission cannot be held responsible for any use that may be made of the information contained therein. V. Vallès research was developed under an FPI-UPC fellowship from Universitat Politècnica de Catalunya (UPC) and funded by the Banco Santander. J. López research was developed under the Margarita Salas postdoctoral fellowship from Ministerio de Universidades (MIU) and funded by the European Union-NextGeneration EU. Support for the research of J.L. Cortina was also received through the "ICREA Academia" recognition for excellence in research funded by the Generalitat de Catalunya and to the Catalan Government (ref. 2021-SGR-596), Spain.

Appendix A. Supplementary material

Supplementary data to this article can be found online at https://doi.org/10.1016/j.seppur.2024.128281.

References

[1] T. Jeppesen, L. Shu, G. Keir, V. Jegatheesan, Metal recovery from reverse osmosis concentrate, J. Clean. Prod. 17 (2009) 703–707, https://doi.org/10.1016/j.jclepro.2008.11.013.
[2] U. Bardi, Extracting minerals from seawater: An energy analysis, Sustainability. 2 (2010) 980–992, https://doi.org/10.3390/su2040980.
[3] A. Shahmansouri, J. Min, L. Jin, C. Bellona, Feasibility of extracting valuable minerals from desalination concentrate: A comprehensive literature review, J. Clean. Prod. 100 (2015) 4–16, https://doi.org/10.1016/j.jclepro.2015.03.031.
[4] European Commission, Critical raw materials | Internal Market, Industry, Entrepreneurship and SMEs, (2023). https://single-market-economy.ec.europa.eu/sectors/raw-materials/areas-specific-interest/critical-raw-materials_en (accessed 5 September 2023).
[5] P. Loganathan, G. Naidu, S. Vigneswaran, Mining valuable minerals from seawater: A critical review, Environm. Sci. Water Res. Technol. 3 (2017) 37–53, https://doi.org/10.1039/c6ew00268d.
[6] B.K. Pramanik, L.D. Nghiem, F.I. Hai, Extraction of strategically important elements from brines: Constraints and opportunities, Water Res. 168 (2020) 115149, https://doi.org/10.1016/j.watres.2019.115149.
[7] B.A. Sharkh, A.A. Al-Amoudi, M. Farooque, C.M. Fellows, S. Ihm, S. Lee, S. Li, N. Voutchkov, Seawater desalination concentrate—a new frontier for sustainable mining of valuable minerals, npj Clean Water 5 (2022) 9, https://doi.org/10.1038/s41545-022-00153-6.
[8] F. Vicari, S. Randazzo, J. López, M. Fernández de Labastida, V. Vallès, G. Micale, A. Tamburini, G. D'Alì Staiti, J.L. Cortina, A. Cipollina, Mining minerals and critical raw materials from bittern: Understanding metal ions fate in saltwork ponds, Sci. Total Environ. 847 (2022) 157544, https://doi.org/10.1016/j.scitotenv.2022.157544.
[9] J.S. Davis, Structure, function and management of the biological system for seasonal solar saltworks, Global NEST J. 2 (2018) 217–226, https://doi.org/10.30955/gnj.000175.
[10] S. Gorjian, F.J. Jamshidian, B. Hosseinqolilou, Feasible Solar Applications for Brines Disposal in Desalination Plants, in: A. Kumar, O. Prakash (Eds.), Solar Desalination Technology, Springer, Singapore, 2019: pp. 25–48. DOI: 10.1007/978-981-13-6887-5.
[11] A. Kumar, G. Naidu, H. Fukuda, F. Du, S. Vigneswaran, E. Drioli, J.H. Lienhard, Metals Recovery from Seawater Desalination Brines: Technologies, Opportunities, and Challenges, ACS Sustain. Chem. Eng. 9 (2021) 7704–7712, https://doi.org/10.1021/acssuschemeng.1c00785.
[12] S.E. Can Sener, V.M. Thomas, D.E. Hogan, R.M. Maier, M. Carbajales-Dale, M. D. Barton, T. Karanfil, J.C. Crittenden, G.L. Amy, Recovery of Critical Metals from Aqueous Sources, ACS Sustain. Chem. Eng. 9 (2021) 11616–11634, https://doi.org/10.1021/acssuschemeng.1c03005.
[13] X. Zhang, W. Zhao, Y. Zhang, V. Jegatheesan, A review of resource recovery from seawater desalination brine, Rev. Environ. Sci. Biotechnol. 20 (2021) 333–361, https://doi.org/10.1007/s11157-021-09570-4.
[14] A. Brewer, J. Florek, F. Kleitz, A perspective on developing solid-phase extraction technologies for industrial-scale critical materials recovery, Green Chem. 24 (2022) 2752–2765, https://doi.org/10.1039/d2gc00347c.
[15] V. Vallès, M. Fernández de Labastida, J. López, J.L. Cortina, Selective recovery of boron, cobalt, gallium and germanium from seawater solar saltworks brines using N-methylglucamine sorbents: Column operation performance, Science of the Total Environment. 923 (2024) 171438, https://doi.org/10.1016/j.scitotenv.2024.171438.
[16] V. Vallès, M. Fernández de Labastida, O. Gibert, A. Leskinen, R. Koivula, J. López, J.L. Cortina, Sorption strategies for recovering critical raw materials: extracting trace elements from saltworks brines, Under Review in Journal of Environmental Chemical Engineering (2024).
[17] V. Vallès, M. Fernández de Labastida, J. López, G. Battaglia, D. Winter, S. Randazzo, A. Cipollina, J.L. Cortina, Sustainable recovery of critical elements from seawater saltworks bitterns by integration of high selective sorbents and reactive precipitation and crystallisation: Developing the probe of concept with on-site produced chemicals and energy, Separ. Purif. Technol. 306 (2023) 122622, https://doi.org/10.1016/j.seppur.2022.122622.
[18] J. Ran, L. Wu, Y. He, Z. Yang, Y. Wang, C. Jiang, L. Ge, E. Bakangura, T. Xu, Ion exchange membrane : New developments and applications, J. Membr. Sci. 522 (2017) 267–291, https://doi.org/10.1016/j.memsci.2016.09.033.
[19] J. Luo, C. Wu, T. Xu, Y. Wu, Diffusion dialysis-concept, principle and applications, J. Membr. Sci. 366 (2011) 1–16, https://doi.org/10.1016/j.memsci.2010.10.028.
[20] R. Gueccia, S. Randazzo, D. Chillura Martino, A. Cipollina, G. Micale, Experimental investigation and modeling of diffusion dialysis for HCl recovery from waste pickling solution, J. Environ. Manage. 235 (2019) 202–212, https://doi.org/10.1016/j.jenvman.2019.01.028.
[21] J. Xu, S. Lu, D. Fu, Recovery of hydrochloric acid from the waste acid solution by diffusion dialysis, J. Hazard. Mater. 165 (2009) 832–837, https://doi.org/10.1016/j.jhazmat.2008.10.064.
[22] J. Xu, D. Fu, S. Lu, The recovery of sulphuric acid from the waste anodic aluminum oxidation solution by diffusion dialysis, Sep. Purif. Technol. 69 (2009) 168–173, https://doi.org/10.1016/j.seppur.2009.07.015.
[23] A. Ruiz-Aguirre, J. Lopez, R. Gueccia, S. Randazzo, A. Cipollina, J.L. Cortina, G. Micale, Diffusion dialysis for the treatment of H2SO4-CuSO4 solutions from electroplating plants: Ions membrane transport characterization and modelling, Sep. Purif. Technol. 266 (2021) 118215, https://doi.org/10.1016/j.seppur.2020.118215.
[24] J. López, R.R. De Oliveira, M. Reig, X. Vecino, O. Gibert, A. De Juan, J.L. Cortina, Acid recovery from copper metallurgical process streams polluted with arsenic by diffusion dialysis, J. Environm. Chem. Eng. 9 (2021) 104692, https://doi.org/10.1016/j.jece.2020.104692.
[25] A. Merkel, L. Čopák, L. Dvořák, D. Golubenko, L. Šeda, Recovery of spent sulphuric acid by diffusion dialysis using a spiral wound module, Int. J. Mol. Sci. 22 (2021) 11819, https://doi.org/10.3390/ijms222111819.
[26] S. Wu, H. Zhu, Y. Wu, S. Li, G. Zhang, Z. Miao, Resourceful treatment of battery recycling wastewater containing H2SO4 and NiSO4 by diffusion dialysis and electrodialysis, Membranes 13 (2023) 570, https://doi.org/10.3390/membranes13060570.
[27]] Fumatech BWT GmbH, Fumasep® FAD-PET-75 Technical Data Sheet, 2020.
[28] U.S. Geological Survey, PHREEQC Version 3.7.3, (2023). https://www.usgs.gov/software/phreeqc-version-3.
[29] M. Laliberté, W.E. Cooper, Model for calculating the density of aqueous electrolyte solutions, J. Chem. Eng. Data 49 (2004) 1141–1151, https://doi.org/10.1021/je0498659.
[30] P. Vanýsek, Ionic conductivity and diffusion at infinite dilution, in: W.M. Haynes (Ed.), CRC Handbook of Chemistry and Physics, 95th ed., 2015: pp. 5–77.
[31] J. Ran, L. Wu, Y. He, Z. Yang, Y. Wang, C. Jiang, L. Ge, E. Bakangura, T. Xu, Ion exchange membranes: New developments and applications, J. Membr. Sci. 522 (2017) 267–291, https://doi.org/10.1016/j.memsci.2016.09.033.
[32] Z. Palatý, H. Bendová, Permeability of a Fumasep-FAD Membrane for Selected Inorganic Acids, Chem. Eng. Technol. 41 (2018) 385–391, https://doi.org/10.1002/ceat.201700595.
[33] T. Luo, S. Abdu, M. Wessling, Selectivity of Ion Exchange Membranes : A Review, J. Membr. Sci. 555 (2018) 429–454, https://doi.org/10.1016/j.memsci.2018.03.051.
[34] J. Luo, C. Wu, Y. Wu, T. Xu, Diffusion dialysis of hydrochloric acid with their salts: Effect of co-existence metal ions, Sep. Purif. Technol. 118 (2013) 716–722, https://doi.org/10.1016/j.seppur.2013.08.014.
[35] Z. Palatý, A. Žáková, Competitive transport of hydrochloric acid and zinc chloride through polymeric anion-exchange membrane, J. Appl. Polym. Sci. 101 (2006) 1391–1397, https://doi.org/10.1002/app.22748.
[36] C. Wei, X. Li, Z. Deng, G. Fan, M. Li, C. Li, Recovery of H2SO4 from an acid leach solution by diffusion dialysis, J. Hazard. Mater. 176 (2010) 226–230, https://doi.org/10.1016/j.jhazmat.2009.11.017.
[37] Z. Palatý, A. Žáková, P. Doleček, Modelling the transport of Cl- ions through the anion-exchange membrane NEOSEPTA-AFN systems HCl/membrane/H2O and HCl-FeCl3/membrane/H2O, J. Membr. Sci. 165 (2000) 237–249, https://doi.org/10.1016/S0376-7388(99)00239-2.
[38] Z. Palatý, A. Žáková, Separation of H2SO4 + CuSO4 mixture by diffusion dialysis, J. Hazard. Mater. 114 (2004) 69–74, https://doi.org/10.1016/j.jhazmat.2004.06.023.
[39] Z. Palatý, A. Žáková, Separation of H2SO4 + ZnSO4 mixture by diffusion dialysis, Desalination 169 (2004) 277–285, https://doi.org/10.1016/j.desal.2004.01.001.
[40] Z. Palatý, A. Žáková, Transport of hydrochloric acid through anion-exchange membrane NEOSEPTA-AFN, J. Membr. Sci. 189 (2001) 205–216, https://doi.org/10.1016/S0376-7388(01)00407-0.
[41] J. Luo, C. Wu, Y. Wu, T. Xu, Diffusion dialysis processes of inorganic acids and their salts: The permeability of different acidic anions, Sep. Purif. Technol. 78 (2011) 97–102, https://doi.org/10.1016/j.seppur.2011.01.028.
[42] J. Luo, C. Wu, Y. Wu, T. Xu, Diffusion dialysis of hydrochloride acid at different temperatures using PPO–SiO2 hybrid anion exchange membranes, J. Membr. Sci. 347 (2010) 240–249, https://doi.org/10.1016/j.memsci.2009.10.029.

[43] Y. Zhao, K. Tang, H. Liu, B. Van der Bruggen, A. Sotto Díaz, J. Shen, C. Gao, An anion exchange membrane modified by alternate electro-deposition layers with enhanced monovalent selectivity, J. Membr. Sci. 520 (2016) 262–271, https://doi.org/10.1016/j.memsci.2016.07.026.

[44] S. Mulyati, R. Takagi, A. Fujii, Y. Ohmukai, H. Matsuyama, Simultaneous improvement of the monovalent anion selectivity and antifouling properties of an anion exchange membrane in an electrodialysis process, using polyelectrolyte multilayer deposition, J. Membr. Sci. 431 (2013) 113–120, https://doi.org/10.1016/j.memsci.2012.12.022.

[45] J. Pan, J. Ding, R. Tan, G. Chen, Y. Zhao, C. Gao, B. Van der Bruggen, J. Shen, Preparation of a monovalent selective anion exchange membrane through constructing a covalently crosslinked interface by electro-deposition of polyethyleneimine, Journal of Membrane Science. 539 (2017) 263–272, https://doi.org/10.1016/j.memsci.2017.06.017.

[46] H. Bendová, L. Dušek, J. Palarčík, Comparison of Anion-Exchange Membranes for Diffusion Dialysis of Mixtures of Acids and Their Iron Salts, Membranes 14 (2024) 6, https://doi.org/10.3390/membranes14010006.

[47] R. Gueccia, D. Winter, S. Randazzo, A. Cipollina, J. Koschikowski, G.D.M. Micale, An integrated approach for the HCl and metals recovery from waste pickling solutions: pilot plant and design operations, Chem. Eng. Res. Des. 168 (2021) 383–396, https://doi.org/10.1016/j.cherd.2021.02.016.

[48] M. Drzazga, A. Chmielarz, G. Benke, K. Leszczyńska-Sejda, M. Knapik, P. Kowalik, M. Ciszewski, Precipitation of germanium from sulphate solutions containing tin and indium using tannic acid, Appl. Sci. 9 (2019) 966, https://doi.org/10.3390/app9050966.